Dalton Transactions

ROYAL SOCIETY OF CHEMISTRY

PAPER

View Article Online
View Journal | View Issue

Cite this: *Dalton Trans.*, 2025, **54**, 17287

From stimuli-responsive emission to a rare aggregation induced emission effect in platinum(II) terpyridyl complexes

Bartosz Zowiślok,[a] Anna Świtlicka,*[a] Anna Maria Maroń,*[a] Krzysztof Cwynar,[a] Marzena Dzida,[a] Marcin Libera,[a] Mariola Siwy,[b] Dorota Kowalska,[c] Sebastian Maćkowski[c] and Ewa Schab-Balcerzak[a,b]

Controlling the spectral properties by changing external factors is a key ingredient in the search for new sensing materials. This work is focused on the photophysical response of [PtCl(*t*BuTPAterpy)] (where *t*BuTPAterpy = 4′-(4-(di(4-*tert*-butylphenyl)amino)phenyl)-2,2′,6′,2″-terpyridine) (**C**). The examined compound was synthesized and characterized by acquiring UV-vis and photoluminescence (PL) spectra in solutions and in the solid state at room and low temperatures. Its photophysical properties were discussed in relation to those of [PtCl(4′-$(CH_3)_2$NPh-terpy)]CF_3SO_3 (**A**) and [PtCl(4′-Ph_2NPh-terpy)]CF_3SO_3 (**B**), which have a similar donor–acceptor structure, in order to emphasise the beneficial features of the studied compound. At room temperature, its photoluminescence is 'ON' in a viscous medium (triacetine), whereas in non-viscous media, no emission signal was observed. The rotation of the substituent may be the factor responsible for the lack of emission in dilute solutions. To support this hypothesis, a series of experiments was performed, which showed that the photoluminescence is switched on under conditions of low temperature, acid–base equilibrium, viscosity and aggregation. Compound **C** exhibits reversible mechanochromism with a colour change from red to brown and an emission shift from 708 nm to 783 nm. PXRD and SEM techniques were employed to support the observation of mechanochromic changes. The attractive solid-state photophysical properties, including reversible mechanochromism and tunable emission, indicate that compound **C** is a promising candidate for exploration for OLED applications.

Received 13th June 2025,
Accepted 30th September 2025

DOI: 10.1039/d5dt01391g

rsc.li/dalton

Introduction

One of the major research trends in fundamental research and practical applications is the tuning – through conscious control – of the photophysical properties of transition metal complexes *via* the manipulation of environmental factors. Significant attention is being given to stimuli-responsive luminescence switching through external perturbations, such as mechanical stress,[1] temperature,[2–4] chemical vapours,[5] and acid–base dependent equilibrium.[5] Piezochromic luminescent materials form a group of compounds that exhibit emission colour changes in response to grinding and pressing. These materials, which respond to external pressure by providing observable signals, are highly desirable due to their potential sensor properties.[4,6] Mechanochromism is the phenomenon in which a material undergoes drastic changes in colour and luminescence that are visible to the naked eye when exposed to mechanical forces such as grinding, cutting, or rubbing.[7,8] The key feature of mechanochromism is its reversibility: the ground compound can be reverted to its original state by exposure to organic vapours; this process can often be repeated for multiple cycles.[9] Several structural factors, such as molecular arrangement, conformational flexibility, and intermolecular interactions, have been considered to explain the origin of mechanochromism.[10] The term 'vapochromic effects' refers to a reversible or irreversible change in the colour and emission of a compound in response to gas and/or vapour adsorption/desorption.[11] Some polypyridine–platinum(II) complexes demonstrate excellent mechanochromic and vapochromic responses upon exposure to chemical vapours such as those of alcohols or hydrocarbons.[9] Within the group of terpy-Pt(II) systems, vapochromic behaviour has been confirmed for [Pt(Cl-terpy)Cl]Cl, (Cl-terpy = 4-chloro-2,2′:6′,2″-terpyridine)[12]

[a]*Institute of Chemistry, University of Silesia, 9 Szkolna Str., 40-006 Katowice, Poland. E-mail: anna.switlicka@us.edu.pl, anna.maron@us.edu.pl*
[b]*Centre of Polymer and Carbon Materials, Polish Academy of Sciences, 34 M. Curie-Sklodowska Str., 41-819 Zabrze, Poland*
[c]*Institute of Physics, Faculty of Physics, Astronomy and Informatics, Nicolaus Copernicus University in Toruń, Grudziądzka Str.5, 87-100 Toruń, Poland*

[Pt(terpy)Cl]PF_6,[13] [Pt(terpy-COOH)Cl]CF_3SO_3 (4′-carboxy-2,2′:6′,2″-terpyridine),[14] [Pt(Nttpy)Cl]$(CF_3SO_3)_2$ (Nttpy = 4′-(*p*-nicotinamide-*N*-methylphenyl)-2,2′:6′,2″-terpyridine),[8] with red-shifts of the emission wavelength being observed for these systems. Mechanochromism and the aggregation induced emission (AIE) effect have been observed less frequently. Importantly, four-coordinated Pt(II) compounds feature square-planar geometry at the metal centre, and thus, their complexes with flat π-type ligands enable distinct stacking arrangements *via* Pt···Pt and π···π interactions, and/or hydrogen bonds.[10,15] This opens a path to AIE and excellent stimuli-responsive luminescence properties.[16–19] Among Pt(II) systems, only a few rare examples respond positively to multiple external stimuli. In the family of terpy-Pt(II) compounds, only [Pt(Nttpy)Cl]$(CF_3SO_3)_2$ and [Pt(terpy-COOH)Cl]CF_3SO_3 have shown two different sensing properties: pH-sensing/vapochromism and vapo-/mechanochromism, respectively [Table S2].

Additionally, due to the structural characteristics of Pt(II) complexes, they are being explored for applications in light-emitting technologies, such as visible light or near-infrared (NIR) emitters. Consequently, the potential of synthesized Pt(II) compounds for OLED and NIR-OLED applications has been tested.[20–26] In the current paper, we focus on a Pt(II) complex (sample **C**) with 4′-(4-(di(4-*tert*-butylphenyl)amino)phenyl)-2,2′,6′,2″-terpyridine (*t*BuTPAterpy). The push–pull organic ligands were previously found to be sensitive to environmental factors, including polarity, viscosity, and acid–base equilibrium, thus displaying rather complex photophysics.[27,28] Here, we develop the knowledge about its chloride Pt(II) coordination compound (compound **C**) in the context of structurally diverse platinum(II) systems with 2,2,6′,2″-terpyridines substituted at the 4′ position with phenyl-linked electron donating groups (**A**–**C**) (Scheme 1). The coordination cation of compound **A** is known from the literature, and its synthesis and photophysical characterization have been reported.[34,35] The present work focuses on platinum(II) complexes with $CF_3SO_3^-$ as the counterion, whereas the previously studied compound involving the cation of **A** was a chloride derivative, and thus is not included in the discussion. To gain a comprehensive understanding of the excited-state processes of the designed compounds, a wide range of spectroscopic techniques was employed, and the data were complemented by theoretical studies (TD-DFT/DFT). The study presented herein centres on the structural and photophysical properties of all three Pt(II) complexes (compounds **A**–**C**), and comprehensive experiments on the selective and reversible luminescence response of compound **C** to external stimuli, such as gentle grinding (mechanochromism), acid–base conditions (pH-dependent luminescence), temperature variation, and the viscosity of the medium. Furthermore, the potential of this compound in the context of the AIE phenomenon as well as OLED technology has been examined.

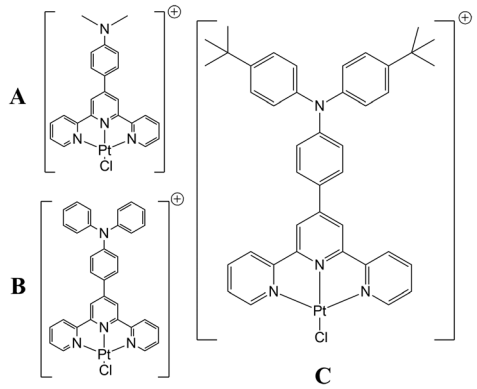

Scheme 1 Structures of the Pt(II) cations (**A**–**C**) employed in this study.

Experimental

Materials

All the reagents used for the syntheses of the coordination compounds were commercially available and were used without further purification. The precursor [$Pt(PhCN)_2Cl_2$] (99% purity) was obtained from Strem Chemicals Inc. and was used without further purification. The 2,2′:6′,2″ terpyridine derivatives were obtained by condensation of 2-acetylpyridine with the corresponding aldehyde [4-(dimethylamino)benzaldehyde] for **A**, 4-(diphenylamino)benzaldehyde for **B**, and 4-(bis(4-(*tert*-butyl)phenyl)amino)benzaldehyde for (**C**) according to literature methods.[29–33] Triethylamine (TEA) and trifluoroacetic acid (TFA) were also obtained from Sigma Aldrich and were used without additional purification.

Preparation of Pt(II) complexes

A suspension of the precursor [$Pt(PhCN)_2Cl_2$] (0.100 g, 0.21 mmol) in acetonitrile (10 mL) was treated with an equimolar amount of $Ag(CF_3SO_3)$ (0.054 g, 0.21 mmol) dissolved in acetonitrile (5 mL). The reaction mixture was heated at 120 °C in a solvatothermal reactor under atmospheric pressure for 16 h and then gradually cooled to 23 °C over another 40 h. After this time, the AgCl precipitate was removed by filtration, and one equivalent of the appropriate ligand [ligand for **A** (74 mg, 0.21 mmol); ligand for **B** (100 mg, 0.21 mmol); ligand in **C** (123 mg, 0.21 mmol)] was added to the filtrate. The reaction mixture was heated in the solvatothermal reactor for an additional 24 h at 130 °C and then gradually cooled for another 40 h with a step of 0.04 °C min^{-1}. In both steps, polypropiolactone (PPL)-lined hydrothermal autoclave reactors were used.

Compound A. Yield: 60% (92 mg). $C_{23}H_{20}N_4ClPt$, CF_3SO_3: C 39.38% H 2.75% N 7.65%; found: C 39.47% H 2.41% N 7.33%; ^{1}H NMR (500 MHz, DMSO) δ 8.88 (s, 1H), 8.84–8.72 (m, 2H), 8.50 (t, J = 7.7 Hz, 1H), 8.12 (d, J = 7.8 Hz, 1H), 7.94–7.87 (m, 1H), 6.90–6.82 (m, 1H), 3.10 (s, 3H). ^{13}C {^{1}H} NMR (126 MHz, DMSO) δ 158.60, 153.72, 152.94, 152.25, 151.24, 142.49, 129.54, 129.15, 126.06, 120.46, 119.88, 118.15, 112.24, 40.25; IR (KBr, cm^{-1}): 3448, 1571, 1479, 1415, 1263, 1161, 1029, 838, 785, 756, 669, 637, 518. HRMS ESI MS, $C_{23}H_{20}N_4ClPt$ $[M]^+$ calculated: 582.1035 Da, found: 582.1028 Da; HRMS ESI MS, $CF_3O_3S^-$ $[M]^+$ calculated: 148.9525 Da, found: 148.9520 Da.

Compound B. Yield: 70% (125 mg). $C_{33}H_{25}N_4ClPt$, CF_3SO_3: C 47.64% H 2.94% N 6.54%; found: C 47.36% H 2.47% N 6.18%; ^{1}H NMR (500 MHz, DMSO) δ 8.88–8.77 (m, 2H), 8.74 (d, J = 7.9 Hz, 1H), 8.49 (td, J = 7.9, 1.5 Hz, 1H), 8.05–7.99 (m, 1H), 7.94–7.87 (m, 1H), 7.47–7.39 (m, 2H), 7.27–7.17 (m, 3H), 7.07 (d, J = 8.9 Hz, 1H). ^{13}C {^{1}H} NMR (126 MHz, DMSO) δ 158.68, 154.42, 152.44, 151.61, 150.96, 146.40, 142.90, 130.42, 129.76, 129.53, 126.29, 126.10, 125.42, 120.73, 120.38; IR (KBr, cm^{-1}): 3448, 1581, 1479, 1415, 1334, 1263, 1161, 1029, 838, 785, 756, 699, 637. HRMS ESI MS, $C_{23}H_{20}N_4ClPt$ $[M]^+$ calculated: 706.1348 Da, found: 706.1327 Da. HRMS ESI MS, $CF_3O_3S^-$ $[M]^+$ calculated: 148.9525 Da, found: 148.9524 Da.

Compound C. Yield: 70% (142 mg). $C_{41}H_{40}N_4ClPt$, CF_3SO_3: calcd C 52.09%, H 4.16%, N 3.66%; found: C 51.93%; H 4.25%; N 3.54%; ^{1}H NMR (500 MHz, DMSO) δ 8.96 (d, J = 5.9 Hz, 2H), 8.86 (s, 2H), 8.79 (d, J = 7.9 Hz, 2H), 8.55 (td, J = 7.9, 1.5 Hz, 2H), 8.06–8.01 (m, 2H), 7.97 (ddd, J = 7.3, 5.6, 1.4 Hz, 2H), 7.47–7.41 (m, 4H), 7.15–7.08 (m, 4H), 7.02 (dd, 2H), 1.32 (s, 18H). ^{13}C {^{1}H} NMR (101 MHz, DMSO) δ 158.25, 153.91, 152.13, 151.19, 150.69, 147.34, 143.20, 142.40, 129.21, 129.02, 128.15, 127.40, 126.59, 125.93, 125.72, 125.26, 119.78, 119.47, 34.25, 31.15. IR (KBr, cm^{-1}): 3450, 1587, 1507, 1479, 1463, 1416, 1330, 1266, 1161, 1030, 830, 1788, 638. HRMS ESI MS, $C_{23}H_{20}N_4ClPt$ $[M]^+$ calculated: 818.2600 Da, found: 818.2573 Da; HRMS ESI MS, $CF_3O_3S^-$ [M]+ calculated: 148.9525 Da, found: 148.9526 Da.

Physical measurements

A Perkin–Elmer CHN-2400 analyzer was used for elemental analyses (C, H, N), and a Bruker 400 MHz spectrometer was used for measuring ^{1}H and ^{13}C{^{1}H} NMR spectra in dimethyl sulfoxide-d^6. IR spectra (4000–400 cm^{-1}/KBr pellets) and electronic absorption spectra (range: 600–250 nm in acetonitrile, glyceryl triacetate (triacetine), dichloromethane; $c = 5 \times 10^{-6}$ mol dm^{-3}) were measured using a Nicolet iS5 FT-IR spectrophotometer and Evolution 220 spectrophotometer, respectively.

The photoluminescence (PL) spectra (in acetonitrile, glyceryl triacetate, dichloromethane; $c = 2.5 \times 10^{-5}$ mol dm^{-3}) were measured using an FLS-980 fluorescence spectrophotometer with a Ushio Xenon short arc lamp (UXL-451-0). The low-temperature (~77 K) emission spectra were measured in an ethanol : methanol mixture (4 : 1) frozen-glass matrix at the temperature of liquid nitrogen with a Dewar assembly. Since no emission was detected in acetonitrile or dichloromethane, time-resolved PL measurements were carried out for glyceryl triacetate solution and solid samples at room temperature, as well as for the frozen-glass sample at low temperature, using the time correlated single photon counting (TCSPC) or multichannel scaling (MCS) methods and the FLS-980 spectrophotometer. The excitation wavelength for room-temperature experiments was obtained using a picosecond pulsed diode laser (EPL–470; Edinburgh Photonics) as the light source, whereas for the frozen-glass sample at low temperature, a 60 W μF920H xenon flashlamp (Edinburgh Photonics) was the light source. A photomultiplier (Hamamatsu, R928P) in cooled housing was the detector. Prior to the analysis of phosphorescence decays, IRF measurements were performed at the excitation wavelengths using a LUDOX® solution as the standard. The decay curves were then fitted using a fitting procedure included in the FLS-980 software to estimate χ^2 in the range 0.989–1.264. The integrating sphere absolute method was used to determine the quantum yields with the pure solvent and Spectralon® as references for solution and solid-state samples, respectively. Each measurement was repeated 5 times with a 0.25 nm step and 0.2 dwell time. The quantum yield values were determined using the FLS-980 software with an average error of 2%. Temperature-dependent emission spectra were recorded in MeOH : EtOH solution (c = 25 μM) using a liquid nitrogen cryostat (Optistat DN, Oxford Instruments) equipped with a Mercury iTC temperature controller (Oxford Instruments).

To collect electroluminescence (EL) spectra, a precise voltage power supply (Gw Instek PSP-405) was applied with the sample fixed to an XYZ stage. Light from the OLED device was collected through a 30 mm lens, focused on the entrance slit (50 μm) of a monochromator (Shamrock SR-303i), and detected using a CCD detector (Andor iDus 12305). Typical acquisition times were equal to 10 seconds. The pre-alignment of the setup was done using a 405 nm laser.

Viscosity was determined with an MCR 302e oscillatory rheometer (Anton Paar, Austria) with cone plate geometry (diameter 49.969 mm, cone angle 1.021°) with a gap width of 0.104 mm. The temperature was maintained with a built-in Peltier system with an accuracy of ±0.01 K. As the samples exhibited Newtonian behaviour, the experiment was conducted at constant shear rate conditions equal to 50 s^{-1} at 298.15 K and 323.15 K. Before every measurement at a selected temperature, the sample was exposed to a shear rate of 50 s^{-1} for 60 s to remove any shear history effect. All results are averages from three independent measurements. Based on the calibration procedure, test runs, measurement procedure, and sample properties, the expanded uncertainty (coverage factor k = 2, confidence level 0.95) for viscosity in this work was estimated to be ±3%.

The microstructure of the samples, combined with their spectral properties, were characterized using a Clara scanning electron microscope (SEM) (Tescan Group, a.s., Czech Republic) and Stellaris 8 light confocal microscope (Leica Microsystems GmbH, Germany). SEM micrographs were obtained from secondary electrons, which were collected using an Everhart–Thornley Detector (ETD) under high vacuum conditions at a 1 kV primary electron acceleration voltage. Confocal analysis was accomplished using a white-light laser.

Devices with the configuration ITO/PEDOT:PSS/complex/Al and ITO/PEDOT:PSS/PVK:PBD:complex/Al were prepared as follows: OSSILA substrates with pixilated ITO anodes were covered with PEDOT:PSS by the spin-coating technique at 5000 rpm for 60 s and annealed for 15 min at 120 °C. Next, the Pt(II) complex or PVK:PBD:complex in chloroform solution was spin-coated at 1000 rpm for 60 s and annealed for 5 min at 100 °C. After annealing, the Al (110 nm) was vacuum-deposited.

Theoretical calculations

DFT calculations were performed using the GAUSSIAN-16 program package.[36] The geometry of the singlet ground state (S_0) was fully optimized without any symmetry restrictions at the DFT level using the PBE1PBE hybrid exchange–correlation functional.[37–40] The calculations were performed using the def2-TZVPD basis set for platinum ions and def2TZVP basis set for other elements.[39–41] Vibrational frequencies were calculated on the basis of the optimized geometry to verify that each geometry was a minimum on the potential energy surface. Absorption properties were calculated using the TD-DFT method on the basis of the optimized ground-state geometries. The polarized continuum model (PCM) was employed to recreate media effects in acetonitrile (CH_3CN).[42–44]

Crystal structure determination and refinement

The single-crystal X-ray diffraction data for compound A were recorded at room temperature using an Oxford Diffraction Gemini A Ultra four-circle diffractometer equipped with an Atlas CCD detector, using graphite-monochromated Mo Kα radiation (λ = 0.71073 Å). Data collection, unit-cell refinement, and reduction were carried out with CrysAlisPro software.[45] The structure was solved by direct methods (SHELXS) and refined on F^2 by full-matrix least-squares using SHELXL-2014.[46] All non-hydrogen atoms were refined anisotropically. Hydrogen atoms were placed in idealized riding positions, with C–H distances fixed at 0.93 Å (aromatic) and 0.96 Å (methyl), and the isotropic displacement parameters were set to U_{iso}(H) = 1.2 U_{eq}(C) (aromatic) or 1.5 U_{eq}(C) (methyl). Crystallographic details for compound A are summarized in Table S1 (SI), and the full data have been deposited with the CCDC (deposition number 2451115). Powder X-ray diffraction (XRPD) measurements for compounds **A** and **C** were performed using a PANalytical Empyrean X-ray diffractometer with Cu-Kα radiation (λ = 1.5418 Å), in which the X-ray tube was operated at 40 kV and 30 mA in the range from 5 to 50°.

Results and discussion

Synthesis and general characterization

The complexes **A–C** were synthesized according to a modification of the synthetic procedure described by Büchner, which was used for the preparation of [Pt(terpy)Cl]X (X = $CF_3SO_3^-$, SbF_6^-).[47–49] In the two-step method, the precursor $[PtCl_2(PhCN)_2]$ was refluxed in acetonitrile with one equivalent of $Ag(CF_3SO_3)$ in order to give the compound $[PtCl(PhCN)_2(CH_3CN)]CF_3SO_3$. After filtration of AgCl, the obtained intermediate complex was used for further synthesis with 4′-(4-(di(4-*tert*-butylphenyl)amino)phenyl)-2,2′,6′,2″-terpyridine (*t*BuTPAterpy), resulting in the formation of compound **C**. Both reactions were implemented in a solvothermal reactor under atmospheric pressure. The synthesis of compounds **A** and **B** was carried out in a similar manner to that of compound **C**. Detailed conditions of the synthetic procedures are described in the Experimental section.

The purity and identity of the compounds were confirmed using elemental analysis and NMR and FT-IR spectroscopies. The IR spectra of the free ligand and Pt(II) complexes show characteristic bands in the range of 1610–1560 cm^{-1} assigned to ν(C=N) and ν(C=C) stretching vibrations. Absorptions assignable to the SO_3 part of the SO_3CF_3 anion are observed at 1266 cm^{-1} ($\nu_a(SO_3)$), 1030 cm^{-1} ($\nu_s(SO_3)$) and 638 cm^{-1} ($\delta_a(SO_3)$) (Fig. S1).[50] The coordination of the tridentate ligand was also confirmed using ^{1}H NMR, $^{13}C\{^1H\}$ NMR and HR-MS techniques (Fig. S2).

Solid state structure of compound A

Complex **A** crystallizes in the monoclinic $P2_1/n$ space group. A perspective view of its molecular structure together with the atom numbering is shown in Fig. 1, while selected bond distances and bond angles are included in Table S2. It is noteworthy that despite many attempts, we were unable to successfully isolate crystalline forms of complexes **B** and **C**.

The platinum(II) centre in the cation $[PtCl[(Me)_2Ph\text{-}terpy]^{2+}]$ displays a distorted square planar coordination defined by one chloride ion and three nitrogen atoms from one molecule of the tridentate terpy derivative. The atoms involved in the coordination around the Pt(II) ion deviate 0.013 Å from the mean plane through the four atoms N(1), N(2), N(3), and Cl(1), while the angles around the metal(II) atom show slight deviations from the ideal 90° and 180°, falling in the ranges [80.4(3)–99.4(2)°] and [161.6(3)–179.4(3)°]. A slight deviation from square planar geometry is also evidenced by Okuniewski's parameter (τ_4') calculated using the following equation:

$$\tau_4' = \frac{\beta - \alpha}{360^\circ - \theta} + \frac{180^\circ - \beta}{180^\circ - \theta}$$

where α and β are the two greatest valence angles, $\alpha < \beta$ and $\theta = \cos^{-1}(-\frac{1}{3}) \approx 109.5^\circ$.[51] The obtained τ_4' value (0.079) is close to

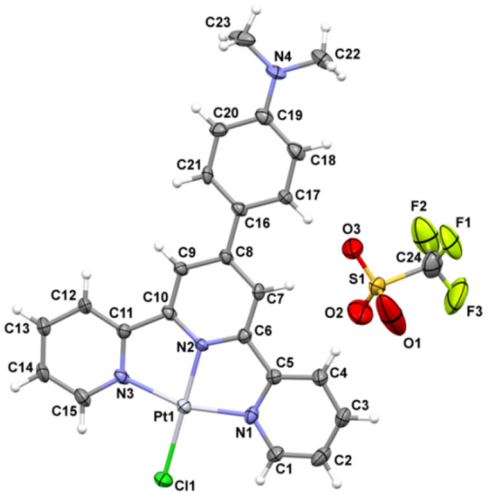

Fig. 1 The molecular structure of compound A with thermal ellipsoids set at 50% probability for non-hydrogen atoms.

the value of 0 expected for ideal square planar geometry, whereas for ideal tetrahedral structures, τ_4' is equal to 1. In comparison to those of related platinum(II) complexes, the Pt–N bond of the outer terpy rings is longer than that of the central pyridyl ring, located at the position *trans* to the Cl anion.[52–54] In complex **A**, the terpy skeleton shows good planarity, and the dihedral angles between the inner and outer rings are 0.96° and 5.83°, respectively, while twist angle for the substituent ring with respect to the central ring of the triimine framework is equal to 3.81°.

The packing analysis (Mercury, 3.10.2 program) shows that neighboring cations of complex **A** are oriented in a head-to-tail manner relative to each other, and the crystal packing of **A** was largely contributed by the intermolecular hydrogen bonds C–H···O and C–H···Cl and π···π stacking (see Fig. S4 and Tables S3, S4 in the SI).[55]

Electronic absorption and emission spectra in solution

The electronic absorption spectra of compounds **A–C** were measured in three solvents of different polarity (ε) and viscosity (η): acetonitrile (ε = 37.5; η = 0.34 cP), dichloromethane (ε = 37.5; η = 0.41 cP), and glyceryl triacetate (triacetin) (ε = 7.1; η = 25 cP). UV-VIS spectra of **A–C** are shown in Fig. S5, and the spectroscopic data for complex **C** and complexes **A–B** are summarized in Table 1 and Table S5 in the SI, respectively. The spectral profiles of compounds **A–C** in acetonitrile are comparable to each other. The vibronically structured high-energy absorption bands can be attributed to spin-allowed π → π* and n → π* intraligand (IL) transitions associated with the coordinated terpyridyl-like ligand.[56,57] The lower-energy absorption with λ_{abs}^{max} in the range of 479–490 nm can be attributed to the CT transition (see TD-DFT calculations below).[58] Comparing the electronic spectra of the compounds **A–C** with those of [PtCl(4′-Phterpy)]TFPB (TFPB = tetrakis[3,5-bis(trifluoromethyl)phenyl]borate), which are known from the literature,[56,57] it can be noted that the low-energy bands of these complexes are bathochromically shifted compared to those of [PtCl(4′-Phterpy)]TFPB.

The longest-wavelength absorption bands of **A–C** in dichloromethane are red-shifted by 34 nm (for **A**), 45 nm (for **B**) and 50 nm (for **C**) with reference to those in acetonitrile solution. The bathochromic shift of the absorption bands accompanying the change of solvent from more-polar CH_3CN to less-polar CH_2Cl_2 indicates that the molecules of the compounds in the ground states are more polar than those in the excited states. Similar behaviour was previously indicated in ref. 56. As can be seen from Table S5, in both acetonitrile and dichloromethane, the maximum of CT absorption for **C** is located at lower energy relative to those of compounds **A** and **B**, which can be attributed to the increase in ILCT character due to the influence of the substituent (see TD-DFT calculation section below). Moreover, compared to those of [Pt(dma-terpy)Cl]CF_3SO_3 and [Pt(pyrr-terpy)Cl]CF_3SO_3 (where dma-terpy = 4′-(dimethylamino)-2,2′:6′,2″-terpyridine, pyrr-terpy = 4′-(pyrrolidin-1-yl)-2,2′:6′,2″-terpyridine)[56] with directly substituted amino groups, it can be seen that the addition of the phenyl linker in the structures of **A–C** results in significant bathochromic shifts of the CT absorption.

Theoretical calculations[36,59] at the DFT/PBE1PBE/DEF2-TZVPD/DEF2-TZVP level of theory were performed in order to understand the nature of the excited state responsible for absorption. The calculated absorption energies associated with their oscillator strengths and major contributions, as well as their assignments to the experimental results, are given in Tables S6–S8 (SI). As shown in Fig. S13 and Table S2 for compound **A**, for example, the structural features are well reproduced by the DFT calculations. The TD-DFT calculated UV-vis absorption spectra shown in Fig. S6–S11 display bathochromic shifts of 945–2258 cm^{-1} with reference to the experimental ones. This discrepancy is quite typical of those reported for long distance charge separated molecules.[60] In order to avoid underestimating the calculated values with respect to the experimental UV-VIS data, as well as due to the differences in the description of the electronic structure of studied complexes, the influence of a few selected functionals (B3LYP, CAM-B3LYP and ωB97X-D) on the results was taken into account, and the results showed that the PBE1PBE functional is an optimal choice (Fig. S12).

In compounds **A–C**, the HOMO level is marginally influenced by the metal atom. The percentage of the PtCl fragment decreases from **A** (3.17%) to **B** (1.55%) to **C** (1.41%). A significant contribution from the Pt(II) ion is found in HOMO−1/HOMO−2. The LUMO levels are dominated by the contribution from 2,2′:6′,2″-terpyridine. Analysing the frontier molecular orbitals, orbital percentage composition, oscillator strength, and transitions assigned to the low-energy absorption band, it can be assumed that there is a balance between ILCT and mixed MLCT/ILCT states, with the first one playing the dominant role. Interestingly, the low-wavelength range of the theoretical absorption spectra of **A–C** is dominated by intense ILCT transitions (HOMO → LUMO and HOMO → L+1

Table 1 Absorption maxima and molar extinction coefficient values together with the photoluminescence data for compound **C**

	UV-vis	Photoluminescence data		
Medium	λ [nm] (ε[dm^3 mol^{-1} cm^{-1}])	λ_{em} [nm]	τ [μs]	Φ [%]
Glyceryl triacetate	512 (10 802), 336 (13 866), 283 (14 461), 263 (14 850)	720	0.9; 2.2	37.0
CH_3CN	490 (16 888), 328 (24 540), 282 (26 396), 258 (24 189)	—		
CH_2Cl_2	540 (21 675), 337 (29 801), 284 (33 926), 263 (31 801)	—		
77 K	—	698	37.2; 75.7	—
Unground solid	247, 353, 447, 479, 526, 561	708	0.1; 2.5; 16.2	11.0
Ground solid	295, 388, 419, 482, 591, 622	783	0.5; 2.5; 43.5	0.8

in **A**; HOMO → LUMO in **B**; HOMO → LUMO in **C**), while the MLCT transitions (H−1 → LUMO in **A** and H−2 → LUMO; H−1 → LUMO in **B**; H−2 → L; H−1 → LUMO in **C**) contribute marginally.

Complex **C** is non-emissive in dilute solutions of acetonitrile and dichloromethane at room temperature. The absence of emission at room temperature was also observed for compounds **A** and **B** in solution. This fact was previously discussed in the case of the tetraphenylborate salt of **A** ([PtCl(4′-NMe_2-Ph-terpy)]BPh_4). Namely, while it shows rather weak photoluminescence at room temperature, it is clearly impeded by the lack of interference between the ^{3}ILCT and ^{3}MLCT excited state, thus favouring non-radiative decay.[61] A possible reason for this effect may be the rotation of the phenyl linker suppressing the communication between excited states and consequently decreasing the phosphorescence properties of the transition metal compound, which presents photophysics connected with the twisted intramolecular charge transfer (TICT) process.

Changing the solvent to the more viscous glyceryl triacetate (*i.e.*, slowing down rotation) results in the appearance of emission for compound **C** (Fig. S5). Excitation at a wavelength corresponding to the lowest energy absorption maximum of [Pt(*t*BuTPAterpy)Cl]CF_3SO_3 in glyceryl triacetate gives rise to one structureless emission band at 720 nm with high quantum efficiency (Φ = 37.0%) (Table 1). The luminescent decay profile was also examined and fitted using a two-exponential-decay function (0.9 μs, 2.2 μs), possibly related to the existence of two excited state species (^{3}ILCT and ^{3}MLCT). Unfortunately, complexes **A–B** display insufficient solubility in glyceryl triacetate to obtain their PL spectra for comparison.

The spectrum of **C** (see Fig. 2) measured at 77 K shows one phosphorescence band, which is blue-shifted in comparison to that of the glyceryl triacetate solution by about 440 cm^{-1}, which confirms the CT nature of the lowest-energy excited state (LEES).[62] Comparison of the low-temperature emission of [PtCl(4′-NMe_2-terpy)]CF_3SO_3 (λ_{PL}, 77 K: 560 nm, 605 nm) as well as that of [PtCl(4′-NMe_2-Ph-terpy)]BPh_4 (λ_{PL}, 77 K: 660 nm (sh), 734 nm) reveals a systematic bathochromic shift, confirming the increase in the ^{3}ILCT character of the LEES in compound **C**.[58,61] However, the low-temperature emission spectra of [PtCl(4′-NMe_2-Ph-terpy)]BPh_4 were affected by an aggregation process.[59] On the contrary, the 77 K spectra of **A** and **C** display similar emission wavelengths (see Table S10), which are red-shifted compared to that of **B**. Taking into account the Hammett's constants for the –CH_3 (−0.17), –Ph (−0.01) and –Ph*t*Bu (−0.07 to −0.10) groups in the structures of **A**, **B** and **C**, respectively, one could expect that **A** and **C** would have similar spectra, whereas the spectrum of **B** might be different.[63] The two-exponential fit of the decay curves at 77 K for **A–C** proves the existence of two excited state species (^{3}ILCT, ^{3}MLCT).

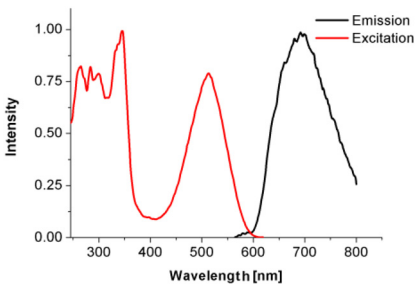

Fig. 2 Emission spectra in rigid MeOH : EtOH (1 : 4 v/v) matrices.

Electronic absorption and emission spectra in the solid state – mechanochromic effect

The solid-state absorption spectra of compound **C** are dominated by one band at 570 nm, which is bathochromically shifted compared to those of compounds **A** and **B**. In light of the well-documented mechanochromic behaviour of platinum (II) complexes and the prior investigation of the TPA motif in this context,[64] the mechanochromic properties of compounds **A–C** were also systematically examined.

Solid state UV-VIS spectra and emission spectra were recorded for each compound twice, *i.e.*, before and after the mechanical grinding of the sample. In the case of compound **C** only, after gentle grinding with a pestle, the red colour of the Pt(II) complex under daylight changed to brown. However, when the ground powder was treated with a few drops of acetonitrile and allowed to dry in air, the complex reverted to its original colour (Fig. 3a). This process was repeated six times without any noticeable degradation of the starting material. The UV-VIS spectrum of the Pt(II) complex after grinding was also measured, and the λ_{abs}^{max} was red-shifted by 1353 cm^{-1} compared to the spectrum before grinding (Fig. 3b). In the case of **A** and **B**, after grinding, a miniscule shift or no shift of the UV-Vis absorption was observed, respectively (see Fig. S16 and PXRD spectra section below) indicating the absence of mechanochromic properties.

In the second step, the mechanoluminescence properties were investigated. No mechanoluminescence properties were

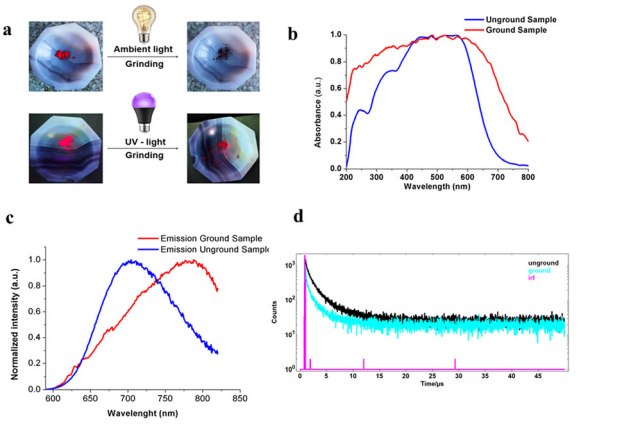

Fig. 3 Visual colour changes under ambient light and under UV light (a); solid absorption spectra before and after grinding (b); emission spectra before and after grinding (c); and the PL decay of sample **C** in the solid state before (black) and after (blue) grinding at RT together with IRF (pink) measured with a 50 μs time window (d).

observed for **A** or **B**, in agreement with the absence of any visible mechanochromism in the absorption spectra. Under UV irradiation at 365 nm, the initial red powder of compound **C** emits bright orange-red light. After the grinding of **C**, the colour of its emission changed slightly to reddish-brown, demonstrating significant and sensitive mechanoluminescence. Upon treatment of the ground powder with a few drops of acetonitrile, the colour and luminescence were quickly recovered. The mechanochromic response was recorded using steady-state visible light absorption spectroscopy together with the visual changes, as presented in Fig. 3a–c.

In agreement with changes in the luminescence colour, the solid-state emission profile of **C** exhibits a red-shift, with λ_{max}, changing from 708 nm to 783 nm in the solids. Based on related studies, the broad, bathochromically shifted emission may be assigned to a metal–metal-to-ligand charge transfer, ^{3}MMLCT, as a result of the formation of Pt···Pt contacts in the newly formed ground aggregates; however, both the unground and ground sample display emission spectra that partially overlap with the monomer emission attributed to ^{3}ILCT/^{3}MLCT excited states.[65,66] The luminescence quantum yield was determined, and a decrease in φ was detected for the solid-state powders upon grinding (Table 1). A decrease in the quantum yield after grinding, accompanied by a significant red-shift of the emission band, has been previously noted for several Pt(II) compounds.[7,65–68] The luminescence decay profiles before and after grinding were studied at room temperature (Fig. 3d). The data for the unground and ground samples differs only marginally (Table 1 and Fig. 3d).

Powder X-ray diffraction (PXRD) analysis was employed to confirm the visual observations as well as the UV-vis absorption and photoluminescence data. As shown in Fig. S17, powder patterns were measured for polycrystalline, ground and unground compounds **A** and **C**. The PXRD pattern of broken crystals of **A** perfectly matched that obtained for the unground sample and the simulated PXRD pattern generated from single-crystal data, confirming the absence of any structural change. On the other hand, the experimental spectra for the ground and unground sample of **C** clearly differ, strongly suggesting conversion from one crystalline form to another. In order to further investigate the structural differences between the ground and unground samples of compounds **A** and **C**, scanning electron microscopy (SEM) was utilized (Fig. 4 and Fig. S18).

The as-synthesized crystals exhibit a rod-like structure (Fig. 4, top), while the ground materials have a cube-like appearance (Fig. 4, bottom). The length of the sides of the cube is similar to the width of the rods formed *via* crystallization, based on the average value determined for 50 objects.

Switching "on" photoluminescence *via* external conditions

The organic *t*BuTPAterpy ligand in the structure of **C** can be considered an interesting combination of the terpy moiety with *t*Bu derivatives of the TPA unit. As a push–pull molecule, it can be sensitive to external conditions such as polarity, viscosity or acid–base equilibrium.[27,28] The terpy unit in the structure of the square planar Pt(II) complex facilitates intramolecular interactions, providing necessary rigidity, while the TPA motive, owing to its non-coplanar structure, can prevent molecular aggregation. The coordination of *t*BuTPAterpy to the Pt(II) ion can open a path to on–off PL properties. In order to explore this phenomenon, the sensitivity of the photoluminescence of **C** to acid–base equilibrium, aggregation processes, and the rigidity and viscosity of the medium was examined.

The experiments involving acid/base equilibrium were conducted for compound **C** in chloroform solution with and without the addition of triethylamine (TEA), and the initial conditions were then restored by the addition of trifluoroacetic acid (TFA) (Fig. 5). The chloroform solution of **C** at room temp-

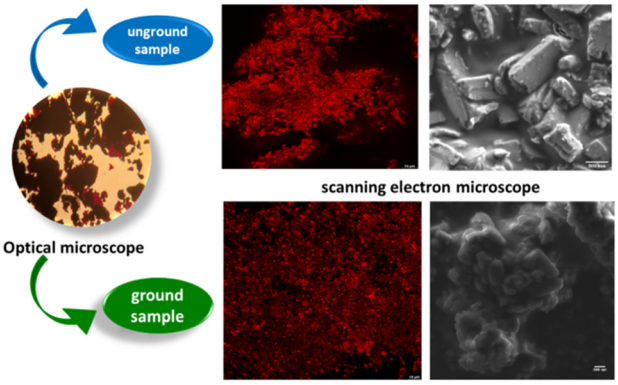

Fig. 4 The morphology of crystalline compound **C** before (top) and after (bottom) grinding. Fluorescence micrographs of compound **C** (left panels) and SEM micrographs of the crystal morphologies of complex **C** (right panels).

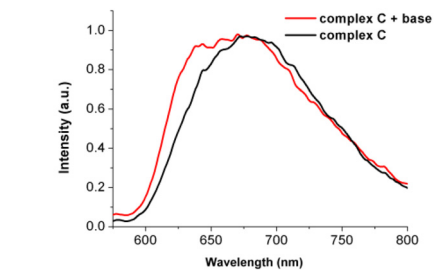

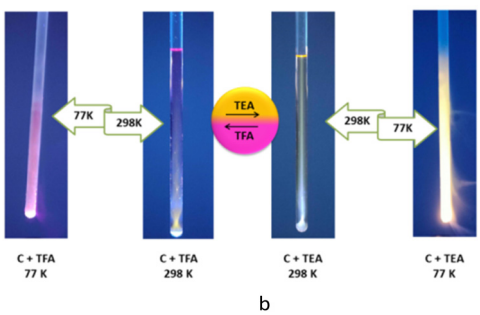

Fig. 5 Emission spectra of **C** in $CHCl_3$ without and with base (TEA) at 77 K (a); and photos of the stimuli-responsive behaviour of a chloroform solution of **C** in an NMR tube (b).

erature is a non-emissive red fluid. After the addition of TEA, its colour changes from red to yellow. After the subsequent addition of an equimolar amount of TFA to the (**C** + TEA) sample, the colour changes again from a yellow to a red (initial) colour. Cooling the solution of (**C** + TEA) to 77 K yields bright yellow emission, shifted to the blue in comparison to that of the complex **C** in $CHCl_3$. An equimolar amount of TFA reverses the process, and the sample exhibits bright pink emission. A similar process can also be observed in dichloromethane. However, for other solvents, such as acetonitrile, DMSO, hexane, and acetone, this phenomenon was not observed.

Generally, square-planar Pt(II) coordination compounds are a powerful tool for studying AIE properties owing to intramolecular interactions (including Pt–Pt, Pt–π, and π–π). However, in the present case, a factor that also has a significant influence on the AIE behaviour is the flexible and sterically hindered substituent of the terpyridine ligand.[69–76]

In order to verify this hypothesis, the PL spectra in THF–H_2O mixtures were acquired. Different fractions of water as a pure solvent (0–90%) were added to the pure THF solution, keeping the same concentration in each solution (2.5×10^{-5} M) (Fig. 6a).

In the pure THF solution, similarly to in the dichloromethane and acetonitrile solutions (see section: Electronic absorption and emission spectra in solution), no emission signal was recorded. This results from the fact that in non-viscous solutions, the di(4-(*tert*-butylphenyl)amino)phenyl substituent in the ligand skeleton can rotate freely, and loses energy *via* undergoing mechanical motion.[77,78] Increasing the percentage of water leads to the formation of aggregates that are visible, even to the naked eye (see Fig. 6A, left side), and a gradual increase in the PL signal due to the AIE phenomenon. One possible reason for the enhancement in the PL is the fact that aggregates can inhibit the mechanical rotation, which

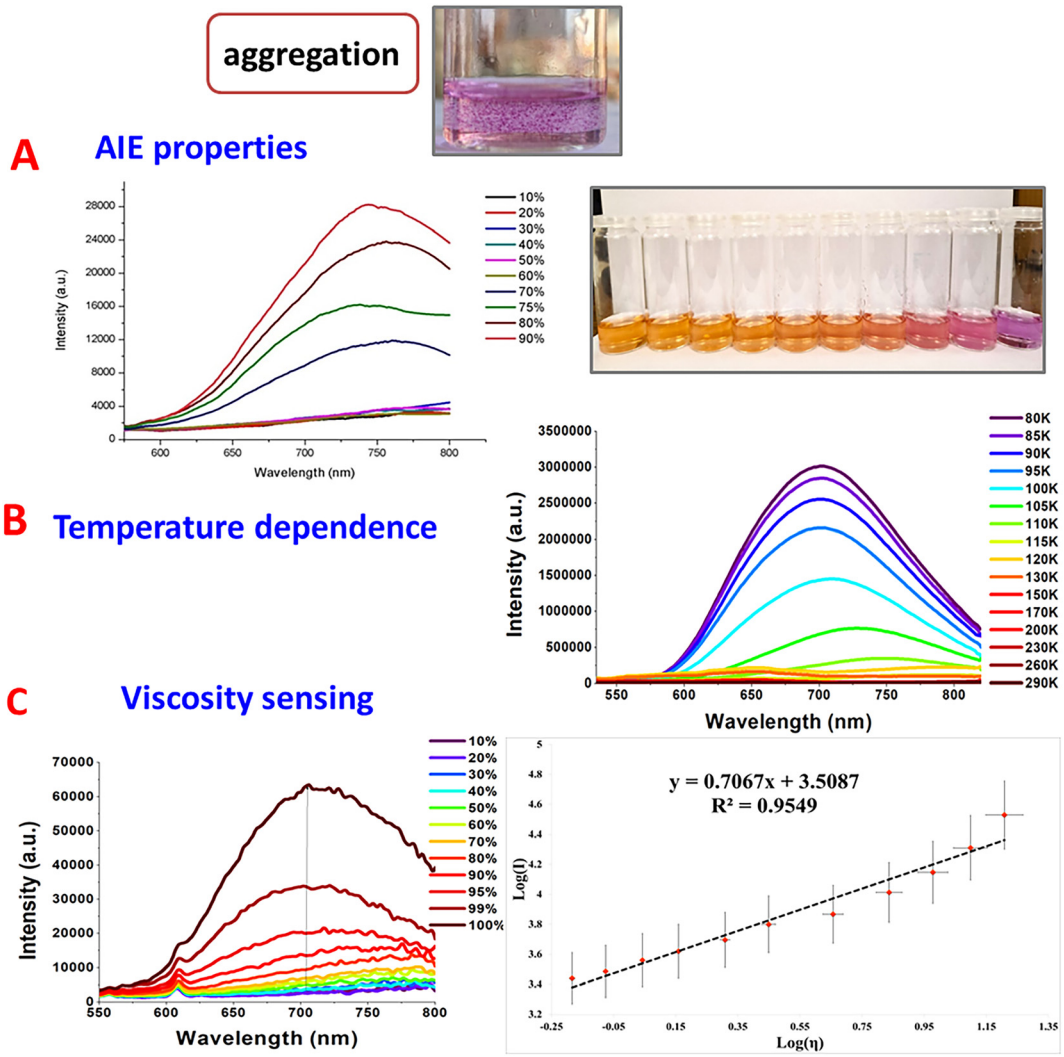

Fig. 6 PL spectra of **C** in THF–H_2O mixtures with different water fractions, together with images showing colour changes from 0% to 90% water fraction in increments of 10% in an open atmosphere (a); PL spectra of **C** in a methanol : ethanol mixture (1 : 4) at different temperatures (b); and emission spectra of **C** in triacetine–methanol mixtures, together with the linear response between log *I* (emission intensity) and log η (viscosity) in glyceryl triacetate–methanol mixtures at different ratios (c).

consequently causes the restoration of the radiative pathway. The emission spectra are almost unchanged in the water fraction range of 10–40%, which suggests strong rotation of the substituent in **C**. When the water fraction is higher than 50%, a dramatic change in the behaviour can be noticed, attributable to effective inhibition of the mechanical motion of the *t*BuTPA chromophore in the coordinated terpy skeleton (Fig. 6a).

Partial verification of whether the rotation of the substituent has an impact on the emitting properties of **C** requires estimation of any rigidochromic effect. The use of a frozen glass matrix, however, affects the emission properties in a dual manner: it almost completely inhibits rotational motion within the molecule, and also prevents solute–solvent rearrangement, thus causing the observed blue-shifts of the CT bands. The latter was discussed in section: Electronic absorption and emission spectra in solution. In order to further explore the thermal and conformational barriers of **C**, its emission spectra in an MeOH : EtOH mixture (1 : 4) over a wide range of temperatures (80–290 K) were recorded. At 80 K, the emission band of **C** is centred at 696 nm (Fig. 6b). Upon increasing the temperature to 120 K, the decrease in emission intensity is accompanied by a red-shift of the emission band at about 1600 cm^{-1}. Above 130 K, the emission band practically vanishes, and the PL spectra in the range 130–290 K show only an artefact band at 650 nm.

As indicated in previous sections, the rotation process can also be inhibited in media with higher viscosity (*e.g.*, in glyceryl triacetate), which may enable the radiative pathway and in turn allow the observation of a strong PL signal. For this reason, and to avoid the observation of both thermal and conformational changes in one experiment, the viscosity sensitivity of the PL spectra of **C** was studied in a methanol–glyceryl triacetate system with increasing fractions of glyceryl triacetate. As the viscosity of the solvent increases, the intensity of the PL emission of the **C** complex is enhanced 32-fold (Fig. 6c, right side). The relation between $\log \eta$ (η – viscosity) and $\log I$ (I – luminescence intensity) exhibits a linear behaviour according to the Förster–Hoffmann equation.[79] The viscosity sensitivity parameter (x) was determined to be 0.7036 (R^2 = 0.9523). These results confirmed that compound **C** can be a good alternative for traditional viscosity sensors and it can sense the viscosity effectively.

Electroluminescence

Taking into account the photoluminescence (PL) properties of the synthesized Pt(II) complex **C**, preliminary investigations of its ability to produce emission under an external voltage were carried out. The electroluminescence (EL) capability of **C** was tested in two kinds of diodes: one with a simple structure, in which the active layer consists of a neat complex (ITO/PEDOT:PSS/Pt(II)complex/Al), and one in a guest–host device bearing

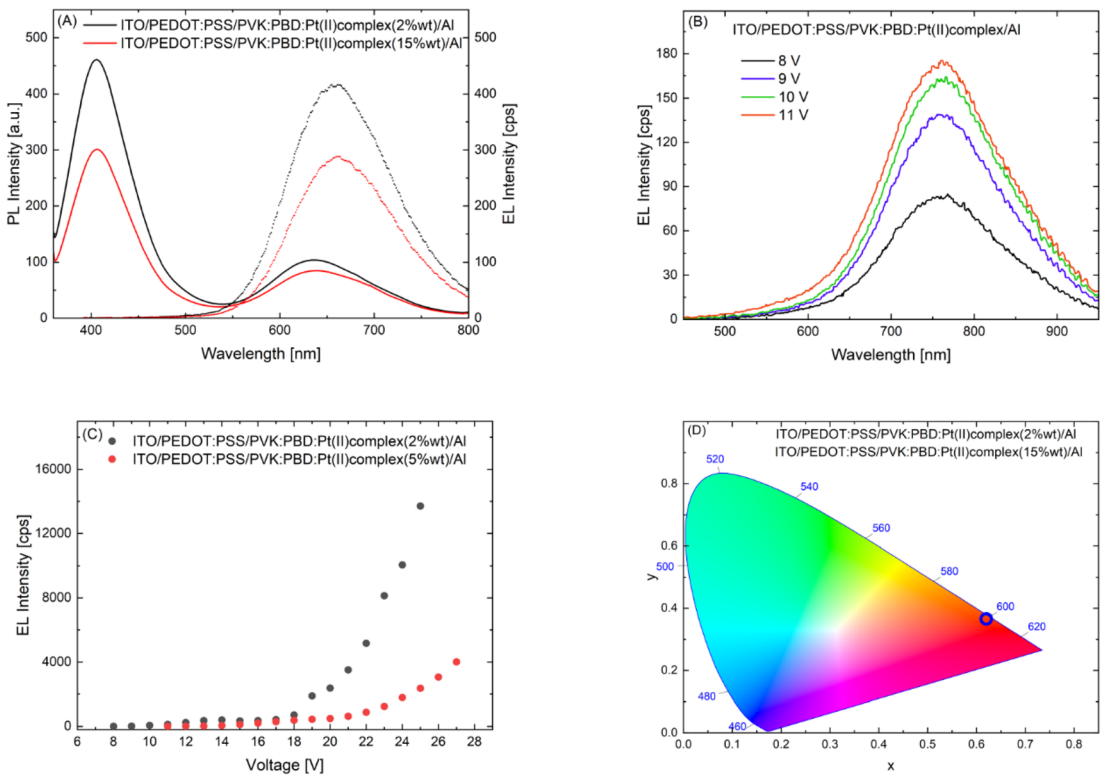

Fig. 7 (a) Photoluminescence (λ_{ex} = 342 nm) and electroluminescence (20 V) spectra for PVK:PBD matrices with increasing amounts of the Pt(II) complex: 2 wt% and 15 wt%, (b) EL spectra of the diode with the neat Pt(II) complex, (c) effects of applied voltage on the EL intensity of the guest–host devices; and (d) chromaticity diagrams of the guest–host diodes (model CIE 1931).

the molecularly dispersed complex (2 and 15% wt) in a binary matrix consisting of poly(9-vinylcarbazole) (PVK) and (2-*tert*-butylphenyl-5-biphenyl-1,3,4-oxadiazole) (PBD) (PVK:PBD, 50:50% by weight) (ITO/PEDOT:PSS/PVK:PBD:Pt(II)complex/Al). Taking into account the principles of the guest–host diode operation, that is, the energy transfer or charge trapping mechanism,[80] the PL spectra obtained from the layers of the same compositions as those used for the diodes were considered. Fig. 7 presents the PL spectra of the PVK:PBD matrix with increasing amounts of the luminophore (Fig. S19).

A PL band originating from the emission of PVK:PBD is observed at shorter wavelengths, in addition to the band ascribed to the PL of the Pt(II) compound. The incomplete quenching of the matrix band indicates that the energy transfer from the PVK:PBD to the luminophore is not complete, mainly due to the weak overlap between the emission spectrum of the host and the absorption spectrum of the guest. The energy transfer can be slightly improved with increasing content of complex **C**, as evidenced by the relative decrease in the PVK:PBD emission band in comparison to the luminophore band.

All the fabricated diodes were emissive, and their EL spectra are presented in Fig. 7a. The EL spectra of the complex in the matrix are compared with the PL registered for the same thin films. The maximum of the electroluminescence band (λ_{EL}) was observed at 760 nm and 670 nm for the diode with the neat complex and with the guest–host configuration, respectively. The λ_{EL} position of the guest–host devices showed no variation with increasing luminophore content. No EL signal of the matrix was seen, which may suggest a charge trapping mechanism rather than energy transfer between the host and the guest. The λ_{EL} of the diodes shifts bathochromically compared to the photoluminescence peak for both types of geometries. The diode based on the neat Pt(II) complex started to emit near-infrared radiation (NIR; $\lambda \geq 700$ nm)[81] at lower voltages compared to the other OLEDs, which emitted red light. The emission intensity of the structure with lower luminophore content in the matrix is significantly higher compared to the diode with 15% wt of the Pt(II) compound. Moreover, the diode with 15% wt. luminophore started to emit light at a lower voltage of ~8 V. Considering the obtained results, it can be concluded that the newly synthesized Pt(II) complex **C** demonstrates potential for NIR-OLED applications. Utilization of the proper matrix may enable shifting the range of the emitted radiation to red light.

Conclusions

In this work, a platinum(II) chloride complex based on a donor–acceptor ligand, namely 4′-(4-(di(4-*tert*-butylphenyl) amino)phenyl)-2,2′,6′,2″-terpyridine (compound **C**), was designed and synthesized with high yields of up to 70%. The identity and purity of the compound were confirmed by studies including elemental analysis, HRMS, FT-IR, and NMR techniques. Its photophysical properties in solution and in the solid phase have been discussed with reference to similar [PtCl(4′-R-terpy)]$^+$ systems, especially [PtCl(4′-$(CH_3)_2$NPh-terpy)]CF_3SO_3 (compound **A**) and [PtCl(4′-Ph_2NPh-terpy)]CF_3SO_3 (compound **B**). The series of complexes **A–C** exhibits a strong single absorption band (ε in the range 10800–21 700 [dm^3 M^{-1}]) in the visible region, which, according to TD-DFT calculations, is mainly assigned to ILCT transition. Excitation within this band of a diluted solution of **C** in non-viscous media (acetonitrile and dichloromethane) yields no emission signal. The same result was obtained in the case of compounds **A** and **B**. The efficient photoluminescence signal (Φ ~37%) is observed only in a diluted solution of **C** in a viscous medium (glyceryl triacetate). A two-exponential fit of the decay time of **C** in this medium indicates the existence of two emitting species (^{3}ILCT and ^{3}MLCT) involved in the luminescence process.

The luminescence switching of **C** was found to be sensitive to a number of external factors: temperature, acid–base equilibrium, viscosity, grinding, and aggregation. We concluded that the rotation of the substituent on the *terpy* skeleton is one of the reasons for the lack of emission in dilute solutions.

The red solid of **C** shows stimuli-responsive properties under mechanical grinding, along with intriguing luminescence responses. Although compounds **A** and **B** are also emissive in the solid phase, no mechanochromism or mechanoluminescence was detected for them. In order to explore the structural differences between ground and unground samples, powder X-ray diffraction and scanning electron microscope techniques were employed. Furthermore, the preliminary tests indicated great potential for the examined complex **C** for both NIR-OLED and OLED applications.

Conflicts of interest

There are no conflicts to declare.

Data availability

The data supporting this article have been included as part of the supplementary information (SI). Supplementary information: additional experimental details: NMR, FT-IR spectra, UV-VIS spectra, luminescent properties in solution, in rigid glass matrix (EtOH : MeOH, 4 : 1 v/v); viscosity in different fractions of triacetin in methanol, PL spectrum of Pt(II) complex, the energies and characters of the selected spin-allowed electronic transition calculated with the TDDFT/PBE1PBE method together with assignment to the experimental absorption bands; composition of frontier molecular orbitals. See DOI: https://doi.org/10.1039/d5dt01391g.

The TD-DFT calculations were carried out in Wroclaw Centre for Networking and Supercomputing (https://www.wcss.wroc.pl).

The data will be available in the The Repository of the University of Silesia (RE-BUŚ) (https://rebus.us.edu.pl/?locale=en).

CCDC 2451115 contain the supplementary crystallographic data for this paper.[82]

Acknowledgements

This research was funded by the National Science Centre of Poland, SONATA grant no. 2020/39/D/ST4/00286. The research activities were co-financed by the funds granted under the Research Excellence Initiative of the University of Silesia in Katowice (POB-2). The background of the graphical abstract was designed by Brgfx/Freepik.

References

1 Y. Ai, Y. Li, M. H.-Y. Chan, G. Xiao, B. Zou and V. W.-W. Yam, *J. Am. Chem. Soc.*, 2021, **143**, 10659.
2 V. W.-W. Yam, K. H.-Y. Chan, K. M.-C. Wong and B. W.-K. Chu, *Angew. Chem., Int. Ed.*, 2006, **45**, 6169.
3 K. H.-Y. Chan, H.-S. Chow, K. M.-C. Wong, M. C.-L. Yeung and V. W.-W. Yam, *Chem. Sci.*, 2010, **1**, 477.
4 M. H.-Y. Chan, S. Y.-L. Leung and V. W.-W. Yam, *J. Am. Chem. Soc.*, 2019, **141**, 12312.
5 Y. Li, L. Chen, Y. Ai, E. Y.-H. Hong, A. K.-W. Chan and V. W. W. Yam, *J. Am. Chem. Soc.*, 2017, **139**, 13858.
6 K. M.-C. Wong, W.-S. Tang, X.-X. Lu, N. Zhu and V. W.-W. Yam, *Inorg. Chem.*, 2005, **44**, 1492.
7 H.-H. Zhang, Q.-Y. Yang, X.-W. Qia, S.-S. Sun, B.-S. Li, D.-S. Zhang, X.-P. Zhang and Z.-F. Shi, *Inorg. Chim. Acta*, 2021, **523**, 120411.
8 A. Han, P. Du, Z. Sun, H. Wu, H. Jia, R. Zhang, Z. Liang, R. Cao and R. Eisenberg, *Inorg. Chem.*, 2014, **53**, 3338.
9 D. Genovese, A. Aliprandi, E. A. Prasetyanto, M. Mauro, M. Hirtz, H. Fuchs, Y. Fujita, H. Uji-I, S. Lebedkin, M. Kappes and L. De Cola, *Adv. Funct. Mater.*, 2016, **26**, 5271.
10 C.-J. Lin, Y.-H. Liu, S.-M. Peng, T. Shinmyozu and J.-S. Yang, *Inorg. Chem.*, 2017, **56**, 4978.
11 E. Li, K. Jie, M. Liu, X. Sheng, W. Zhu and F. Huang, *Chem. Soc. Rev.*, 2020, **49**, 1517.
12 P. Du, *Inorg. Chim. Acta*, 2010, **363**, 1355.
13 R. Zhang, Z. Liang, A. Han, H. Wu, P. Du, W. Lai and R. Cao, *CrystEngComm*, 2014, **16**, 5531.
14 A. Kobayashi, S. Oizumi, Y. Shigeta, M. Yoshida and M. Kato, *Dalton Trans.*, 2016, **45**, 17485.
15 C.-Y. Lien, Y.-F. Hsu, Y.-H. Liu, S.-M. Peng, T. Shinmyozu and J.-S. Yang, *Inorg. Chem.*, 2020, **59**, 11584.
16 S. S. Pasha, P. A. S. Dash, G. Kaur, D. Banerjee, R. Chowdhury, N. Rath, A. R. Choudhury and I. R. Laskar, *RSC Adv.*, 2014, **4**, 50549.
17 C.-J. Lin, Y.-H. Liu, S.-M. Peng, T. Shinmyozu and J.-S. Yang, *Inorg. Chem.*, 2017, **56**, 4978.
18 J. Wu, B. Xu, Y. Xu, L. Yue, J. Chen, G. Xie and J. Zhao, *Inorg. Chem.*, 2023, **62**, 19142.
19 A. Lázaro, R. Bosque, J. S. Ward, K. Rissanen, M. Crespo and L. Rodríguez, *Inorg. Chem.*, 2023, **62**, 2000.
20 L. Huang, C. D. Park, T. Fleetham and J. Li, *Appl. Phys. Lett.*, 2016, **109**, 233302.
21 P. L. dos Santos, P. Stachelek, Y. Takeda and P. Pander, *Mater. Chem. Front.*, 2024, **8**, 1731.
22 A. Üngördü, *Int. J. Quantum Chem.*, 2023, **123**, e27208.
23 Y.-C. Wei, K.-H. Kuo, Y. Chi and P.-T. Chou, *Acc. Chem. Res.*, 2023, **56**, 589.
24 M. Ibrahim-Ouali and F. Dumur, *Molecules*, 2019, **24**, 1412.
25 Y. Sun, B. Liu, Y. Guo, Z. Feng, G. Zhou, Z. Chen and X. Yang, *Org. Electron.*, 2021, **91**, 106101.
26 M. A. Baldo, D. F. O'Brien, Y. You, A. Shoustikov, S. Sibley, M. E. Thompson and S. R. Forrest, *Nature*, 1998, **395**, 151.
27 A. M. Maroń, O. Cannelli, E. C. Socie, P. Lodowski and B. Machura, *Molecules*, 2022, **27**, 7071.
28 A. M. Maron, O. Cannelli, E. C. Socie, P. Lodowski, M. Oppermann, B. Machura and M. Chergui, *Phys. Chem. Chem. Phys.*, 2024, **26**, 6265.
29 J. Palion-Gazda, B. Machura, T. Klemens, A. Szlapa-Kula, S. Krompiec, M. Siwy, H. Janeczek, E. Schab-Balcerzak, J. Grzelak and S. Maćkowski, *Dyes Pigm.*, 2019, **166**, 283.
30 A. M. Maron, A. Szłapa-Kula, M. Matussek, R. Kruszyński, M. Siwy, H. Janeczek, J. Grzelak, S. Mackowski, E. Schab-Balcerzak and B. Machura, *Dalton Trans.*, 2020, **49**, 4441.
31 A. Maroń, A. Szlapa, T. Klemens, S. Kula, B. Machura, S. Krompiec, J. G. Małecki, A. Świtlicka-Olszewska, K. Erfurt and A. Chrobok, *Org. Biomol. Chem.*, 2016, **14**, 3793.
32 U. Resch-Genger, Y. Q. Li, J. L. Bricks, V. Kharlanov and W. Rettig, *J. Phys. Chem. A*, 2006, **110**, 10956.
33 W. Spahni and G. Calzagerri, *Helv. Chim. Acta*, 1984, **67**, 450.
34 X. Han, L.-Z. Wu, G. Si, J. Pan, Q.-Z. Yang, L.-P. Zhang and C.-H. Tung, *Chem. – Eur. J.*, 2007, **13**, 1231.
35 A. Maroń, K. Czerwińska, J. G. Małecki, B. Machura, A. Szłapa-Kula and S. Krompiec, *ChemistrySelect*, 2017, **2**, 1071.
36 M. J. Frisch, G. W. Trucks, H. B. Schlegel, G. E. Scuseria, M. A. Robb, J. R. Cheeseman, G. Scalmani, V. Barone, G. A. Petersson, H. Nakatsuji, X. Li, M. Caricato, A. Marenich, J. Bloino, B. G. Janesko, R. Gomperts, B. Mennucci, H. P. Hratchian, J. V. Ortiz, A. F. Izmaylov, J. L. Sonnenberg, D. Williams-Young, F. Ding, F. Lipparini, F. Egidi, J. Goings, B. Peng, A. Petrone, T. Henderson, D. Ranasinghe, V. G. Zakrzewski, J. Gao, N. Rega, G. Zheng, W. Liang, M. Hada, M. Ehara, K. Toyota, R. Fukuda, J. Hasegawa, M. Ishida, T. Nakajima, Y. Honda, O. Kitao, H. Nakai, T. Vreven, K. Throssell, J. A. Montgomery Jr, J. E. Peralta, F. Ogliaro, M. Bearpark, J. J. Heyd, E. Brothers, K. N. Kudin, V. N. Staroverov, T. Keith, R. Kobayashi, J. Normand, K. Raghavachari, A. Rendell, J. C. Burant, S. S. Iyengar, J. Tomasi, M. Cossi, J. M. Millam, M. Klene, C. Adamo, R. Cammi, J. W. Ochterski, R. L. Martin, K. Morokuma, O. Farkas, J. B. Foresman, and D. J. Fox, *Gaussian 09, Revision A.02*, Gaussian, Inc., Wallingford CT, 2016.

37 J. P. Perdew, K. Burke and M. Ernzerhof, *Phys. Rev. Lett.*, 1996, **77**, 3865.
38 C. Adamo and V. Barone, *J. Chem. Phys.*, 1999, **110**, 6158.
39 F. Weigend and R. Ahlrichs, *Phys. Chem. Chem. Phys.*, 2005, **7**, 3297.
40 D. Rappoport and F. Furche, *J. Chem. Phys.*, 2010, **133**, 134105.
41 D. Andrae, U. Häußermann, M. Dolg, H. Stoll and H. Preuß, *Theor. Chim. Acta*, 1990, **77**, 123.
42 E. Cancès, B. Mennucci and J. Tomasi, *J. Chem. Phys.*, 1997, **107**, 3032.
43 B. Mennucci and J. Tomasi, *J. Chem. Phys.*, 1997, **106**, 5151.
44 M. Cossi, V. Barone, B. Mennucci and J. Tomasi, *Chem. Phys. Lett.*, 1998, **286**, 253.
45 Oxford Diffraction, *CrysAlis PRO*, Oxford Diffraction Ltd, Yarnton, England, 2011.
46 G. M. Sheldrick, *Acta Crystallogr., Sect. C: Struct. Chem.*, 2015, **71**, 3.
47 R. Buchner, J. S. Field and R. J. Haines, *Inorg. Chem.*, 1997, **36**, 3952.
48 R. Büchner, C. T. Cunningham, J. S. Field, R. J. Haines, D. R. McMillin and G. C. Summerton, *J. Chem. Soc., Dalton Trans.*, 1999, 711.
49 G. Annibale, M. Brandolisio and B. Pitteri, *Polyhedron*, 1995, **14**, 451; S. C. Dhara, *Indian J. Chem.*, 1970, **8**, 193.
50 G. A. Lawrance, *Chem. Rev.*, 1986, **86**, 17.
51 A. Okuniewski, D. Rosiak, J. Chojnacki and B. Becker, *Polyhedron*, 2015, **90**, 47.
52 K. Choroba, B. Machura, A. Szlapa-Kula, J. G. Malecki, L. Raposo, C. Roma-Rodrigues, S. Cordeiro, P. V. Baptista and A. R. Fernandes, *Eur. J. Med. Chem.*, 2021, **218**, 113404.
53 H.-K. Yip, L.-K. Cheng, K.-K. Cheung and C.-M. Che, *J. Chem. Soc., Dalton Trans.*, 1993, 2933.
54 R. Buchner, C. T. Cunningham, J. S. Field, R. J. Haines, D. R. McMillin and G. C. Summerton, *J. Chem. Soc., Dalton Trans.*, 1999, 711.
55 C. F. Macrae, I. J. Bruno, J. A. Chisholm, P. R. Edgington, P. McCabe, E. Pidcock, L. Rodriguez-Monge, R. Taylor, J. van de Streek and P. A. Wood, *J. Appl. Crystallogr.*, 2008, **41**, 466.
56 J. F. Michalec, S. A. Bejune, D. G. Cuttel, G. C. Summerton, J. A. Gertenbach, J. S. Field, R. J. Haines and D. R. McMillin, *Inorg. Chem.*, 2001, **40**, 2193.
57 J. F. Michalec, S. A. Bejune and D. R. McMillin, *Inorg. Chem.*, 2000, **39**, 2708.
58 L. M. Hight, M. C. McGuire, Y. Zhang, M. A. Bork, P. E. Fanwick, A. Wasserman and D. R. McMillin, *Inorg. Chem.*, 2013, **52**, 8476.
59 B. P. Pritchard, D. Altarawy, B. Didier, T. D. Gibson and T. L. Windus, *J. Chem. Inf. Model.*, 2019, **59**(11), 4814.
60 T. Klemens, A. Świtlicka, A. Szlapa-Kula, S. Krompiec, P. Lodowski, A. Chrobok, M. Godlewska, S. Kotowicz, M. Siwy, K. Bednarczyk, M. Libera, S. Maćkowski, T. Pędziński, E. Schab-Balcerzak and B. Machura, *Appl. Organomet. Chem.*, 2018, **32**, e4611.
61 A. M. Maroń, K. Choroba, J. G. Małecki, S. Kula and E. Malicka, *Polyhedron*, 2020, **182**, 114502.
62 A. Baschieri, L. Sambri, I. Gualandi, D. Tonelli, F. Monti, A. D. Esposti and N. Armaroli, *RSC Adv.*, 2013, **3**, 6507.
63 A. Yett and P. R. Rablen, *J. Phys. Org. Chem.*, 2023, **36**, e4436.
64 P. S. Hariharan, V. K. Prasad, S. Nandi, A. Anoop, D. Moon and S. P. Anthony, *Cryst. Growth Des.*, 2017, **17**, 146.
65 Y. Nishiuchi, A. Takayama, T. Suzuki and K. Shinozaki, *Eur. J. Inorg. Chem.*, 2011, 1815.
66 D. Genovese, A. Aliprandi, E. A. Prasetyanto, M. Mauro, M. Hirtz, H. Fuchs, Y. Fujita, H. Uji-I, S. Lebedkin, M. Kappes and L. De Cola, *Adv. Funct. Mater.*, 2016, **26**, 5271.
67 L. Gao, J. Ni, M. Su, J. Kang and J. Zhang, *Dyes Pigm.*, 2019, **162**, 231.
68 J. Ni, X. Zhang, Y.-H. Wu, L.-Y. Zhang and Z.-N. Chen, *Chem. – Eur. J.*, 2011, **17**, 1171.
69 H.-H. Zhang, Q.-Y. Yang, X.-W. Qi, S.-S. Sun, B.-S. Li, D.-S. Zhang, X.-P. Zhang and Z.-F. Shi, *Inorg. Chim. Acta*, 2021, **523**, 120411.
70 M. Krikorian, S. Liu and T. M. Swager, *J. Am. Chem. Soc.*, 2014, **136**, 2952.
71 T. Abe, T. Itakura, N. Ikeda and K. Shinozaki, *Dalton Trans.*, 2009, 711.
72 N. Kitani, N. Kuwamura, T. Tsukuda, N. Yoshinari and T. Konno, *Chem. Commun.*, 2014, **50**, 13529.
73 K. Ohno, S. Yamaguchi, A. Nagasawa and T. Fujihara, *Dalton Trans.*, 2016, **45**, 5492.
74 C.-Y. Lien, Y.-F. Hsu, Y.-H. Liu, S.-M. Peng, T. Shinmyozu and J.-S. Yang, *Inorg. Chem.*, 2020, **59**, 11584.
75 L. Gao, J. Ni, M. Su, J. Kang and J. Zhang, *Dyes Pigm.*, 2019, **165**, 231.
76 T. Seki and R. Ishikawa, *Chem. – Eur. J.*, 2025, **31**, e202404241.
77 V. Sicilia, L. Arnal, D. Escudero, S. Fuertes and A. Martin, *Inorg. Chem.*, 2021, **60**(16), 12274.
78 L. Xu, Y. Zou, M. Zeng, S. Duan, K. Wu, R. Han and L. Liu, *ACS Food Sci. Technol.*, 2022, **2**, 49.
79 T. Förster and G. Z. Hoffmann, *Z. Phys. Chem.*, 1971, **75**, 63.
80 K. Kotwica, P. Bujak, D. Wamil, A. Pieczonka, G. Wiosna-Salyga, P. A. Gunka, T. Jaroch, R. Nowakowski, B. Luszczynska, E. Witkowska, I. Głowacki, J. Ulanski, M. Zagorska and A. Pron, *J. Phys. Chem. C*, 2015, **119**, 10700.
81 M. Ibrahim-Ouali and F. Dumur, *Molecules*, 2019, **24**, 1412.
82 CCDC 2451115: Experimental Crystal Structure Determination, 2025, DOI: 10.5517/ccdc.csd.cc2n8l7s.